

Assessing the possible superconductivity in doped perovskite hydride KMgH_3 : Effects of lattice anharmonicity and spin fluctuations

Shaocong Lu^{1,*}, Ryosuke Akashi², Mitsuaki Kawamura³, and Shinji Tsuneyuki¹

¹*Department of Physics, The University of Tokyo, Hongo, Bunkyo-ku, Tokyo 113-0033, Japan*

²*Quantum Materials and Application Research Center,
National Institutes for Quantum Science and Technology,
2-10, Ookayama, Meguro-ku, Tokyo 152-0033, Japan and*

³*Information Technology Center, The University of Tokyo, Tokyo, Tokyo 113-8658, Japan*

(Dated: November 18, 2024)

The superconducting properties of uniformly hole-doped perovskite hydride KMgH_3 with varying doping concentration and lattice parameter corresponding to different pressures were investigated from first principles. The superconducting transition temperature (T_c) was predicted from the density functional theory for superconductors (SCDFT), where the effects of lattice anharmonicity and spin-fluctuation were considered and examined. Although lattice anharmonicity tends to suppress superconductivity around the edge of dynamical stability, where the phase is stabilized due to anharmonic effects, T_c is enhanced. In the hole-doped KMgH_3 , substantial spin-fluctuation (SF) effects were discovered, which counters the phonon-mediated pairing and decreases T_c . Such anomalously strong SF is evaluated for similar hydrides, where the hydrogen 1- s bands are isolated at the Fermi level, and its correlation with the electronics density of states was explored.

I. INTRODUCTION

Hydrogen-rich compounds, along with metallic hydrogen, have long been predicted to be promising candidates for realizing high-temperature superconductivity[1–3]. The discovery of superconductivity in sulfur hydride under pressure in 2015[4] again stimulated the enthusiasm for hydride superconductors. However, hydride superconductors which exhibit high transition temperatures (T_c) almost inevitably require a high pressure (e.g., $T_c \sim 203$ K for H_3S under 200 GPa[4], $T_c \sim 260$ (250) K for LaH_{10} under 200 (170) GPa[5, 6], $T_c \sim 224$ (220) K for YH_6 under 166 (183) GPa[7, 8]). Despite being a challenging task, searching for hydride superconductors that retain a moderate value of T_c at a much lower or even near ambient pressure is still tempting. So far, some predictions on ambient pressure hydride superconductors have been proposed, such as $T_c \sim 54$ K for metastable Al_4H , which adopts a perovskite-like crystal structure[9], and T_c between 45K to 80K for the family of Mg_2XH_6 compounds, where $X = \text{Rh}, \text{Ir}, \text{Pd}$ or Pt [10].

The theory of conventional superconductors was first given by Bardeen, Cooper, and Schrieffer[11] (BCS theory), according to which the superconducting transition temperature T_c can be estimated from

$$T_c = \Theta_D \exp\left(-\frac{1}{N(\epsilon_F)V}\right), \quad (1)$$

where Θ_D , $N(\epsilon_F)$, and V denote the Debye temperature, electronic density of states (DOS) at the Fermi level, and the pairing interaction, respectively. Based on the BCS theory, materials with larger DOS at the Fermi surface

and stronger lattice vibrations are thought to possibly have a higher T_c . So far, much effort has been put into the prediction of novel hydride superconductors, developing high-throughput screening or machine learning models for the prediction relying on the database composed of materials satisfying these two conditions[12–15].

In this paper, we assess the possible superconductivity in hole-doped perovskite KMgH_3 (Fig. 1). Studies on superconducting perovskite hydrides were few, possibly due to the lack of stability in metallic perovskite hydrides. Yagyu *et al.* measured T_c of APdH_{3-x} ($A = \text{Sr}, \text{Ba}$), only to find out they do not exceed 2K[16]. Cerqueira *et al.* predicted the T_c of KCaH_3 , a metallic perovskite hydride at ambient pressure, to be 23.4K from the density functional theory for superconductors (SCDFT)[17]. Although KMgH_3 is a known compound[18], the superconductivity possibility of it brought by doping has not yet been explored. The parent compound KMgH_3 is an insulator, while its valence states are wholly formed by the hydrogen 1 s orbitals. The hole doping is intriguing in that it should realize the metallic state strongly coupling to the hydrogen vibrations. Perovskite oxyhydrides ATiO_2H ($A = \text{K}, \text{Rb}, \text{Cs}$), which also share similar valence

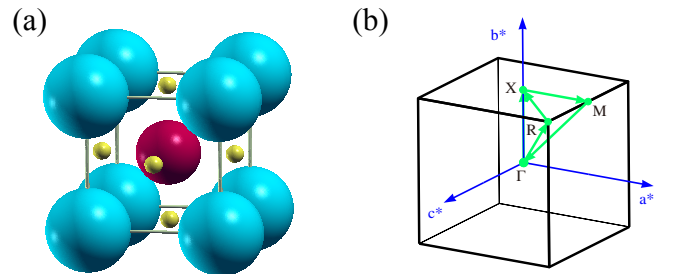


FIG. 1. (a) Crystal structure of perovskite hydride KMgH_3 . The blue, red, and yellow balls represent K, Mg, H atoms respectively. (b) Illustration of the Brillouin zone.

* shaocong.lu@phys.s.u-tokyo.ac.jp

features, have been predicted to show the hole-doping induced superconductivity that coexists with nonzero polarization[19]. Such kinds of oxyhydrides were also reported to have been synthesized[20–23]. The undoped KMgH_3 already shows a excellent stability from ambient pressure to 100GPa, and its highest optical phonon branches can reach around $1,300 \text{ cm}^{-1}$ at ambient pressure.

Despite all the conditions favoring high T_c , hydride superconductors may face some intrinsic drawbacks. Hydrides usually feature strong lattice vibrations, giving rise to large lattice anharmonicity[24, 25], which impact superconductivity[26–29]. Errea *et al.* reported that electron-phonon coupling is reduced by approximately 30% in H_3S under pressure[28], while Sano *et al.* showed that anharmonicity reduces the T_c of H_3S under 250 GPa by 12%[26]. Errea *et al.* also claimed that for palladium hydrides, accounting for anharmonicity reduces the predicted T_c from 47 K to 5 K, in better agreement with experimental values[27]. As a matter of fact, lattice anharmonicity in the PdH system has been extensively studied and is thought to be one of the reasons for the inverse isotope effect[30–32]. Nevertheless, apart from its influence on T_c , anharmonicity is also known to possibly stabilize crystal structures. Errea *et al.* suggested that lattice anharmonicity is the key to the phase stability of $Fm\bar{3}m$ LaH_{10} under pressures between 129 GPa to 214 GPa[33], and $Im\bar{3}m$ H_3S at 155 GPa[34].

In addition, we raise the potential importance of spin fluctuation (SF) in the hydride metals. SF is considered to play against the phonon-mediated pairing between electrons, as the ferromagnetic correlation induced by the exchange coupling tends to destroy the Cooper pairs in the singlet state[35]. In some transition metals with anomalously high magnetic susceptibility, T_c 's predicted from a phonon-mediated pairing mechanism are known to yield overestimated values, which are assumed to be a consequence of neglecting the SF effects in these metals[35–37]. Some of the authors of this paper have shown in their previous study within the SCDFt framework that in elementary superconductors, SF reduces T_c [38, 39]. The T_c reduction was substantial in $3d$ systems like vanadium. According to the degree of the orbital radius, the hydride metals, formed by the extremely localized $1s$ orbital, are likely to suffer from strong SF. Nevertheless, the SF-induced reduction of T_c in hydride superconductors has rarely been investigated, and, to our knowledge, there appears to be no paper on this matter, as the effects are considered trivial. In this paper, we will show a quantitative examination of such effects on hydride superconductors in which the conduction bands are mainly isolated hydrogen bands using the hole-doped KMgH_3 as an example.

In this work, we present a comprehensive study on the stability and superconductivity of hole-doped KMgH_3 from first principles. By systematic examinations across different lattice parameters and doping levels, and taking into account the effects of lattice anharmonicity and SF

in the meantime, we hope to find the optimal conditions for T_c in this material, and to get a deeper understanding of hydride superconductors.

II. COMPUTATIONAL METHODS

The overall study was based on the Eliashberg theory[40] for the conventional phonon-mediated superconductors with the Migdal approximation[41]. T_c were estimated from McMillan-Allen-Dynes's formula (MAD)[42–44]:

$$T_c = \frac{f_1 f_2}{1.2} \exp \left[-\frac{1.04(1+\lambda)}{\lambda - \mu^* - 0.62\lambda\mu^*} \right], \quad (2)$$

$$\omega_{\log} = \exp \left[\frac{2}{\lambda} \int_0^\infty \frac{d\omega}{\omega} \alpha^2 F(\omega) \ln \omega \right], \quad (3)$$

$$\lambda = 2 \int_0^\infty \frac{d\omega}{\omega} \alpha^2 F(\omega), \quad (4)$$

where ω_{\log} is the logarithmic average of phonon frequencies, μ^* denotes the effective Coulomb repulsion, and f_1 and f_2 are the strong-coupling correction factor and the shape correction factor, respectively, which are defined in the following fashion:

$$f_1 = \left[1 + \left(\frac{\lambda}{\Lambda_1} \right)^{3/2} \right]^{1/3}, \quad (5)$$

$$f_2 = 1 + \frac{(\bar{\omega}_2/\omega_{\log} - 1)\lambda^2}{\lambda^2 + \Lambda_2^2}, \quad (6)$$

with the two parameter Λ_1 and Λ_2 defined as:

$$\Lambda_1 = 2.46(1 + 3.8\mu^*), \quad (7)$$

$$\Lambda_2 = 1.82(1 + 6.3\mu^*) \left(\frac{\bar{\omega}_2}{\omega_{\log}} \right), \quad (8)$$

and $\bar{\omega}_2$ denotes the 2nd order average of phonon frequencies:

$$\bar{\omega}_2 = \left[\frac{2}{\lambda} \int_0^\infty d\omega \alpha^2 F(\omega) \omega \right]^{\frac{1}{2}}. \quad (9)$$

$\alpha^2 F(\omega)$ is the isotropic version of the Eliashberg spectral function:

$$\alpha^2 F(\omega) = \frac{1}{N(\epsilon_F)} \int \frac{d\mathbf{k}d\mathbf{q}}{\Omega_{\text{BZ}}} \sum_{m\nu\nu'} |g_{m\nu\nu'}(\mathbf{k}, \mathbf{q})| \delta(\epsilon_{n\mathbf{k}} - \epsilon_F) \times \delta(\epsilon_{m\mathbf{k}+\mathbf{q}} - \epsilon_F) \delta(\hbar\omega_{\mathbf{q}\nu} - \hbar\omega), \quad (10)$$

where ϵ is the Kohn-Sham eigenvalues, $\omega_{\mathbf{q}\nu}$ denotes the phonon frequency with crystal momentum \mathbf{q} in the branch ν , and $g_{m\nu\nu'}(\mathbf{k}, \mathbf{q})$ is the electron-phonon matrix element. To avoid the artificial divergence occurring in the integral of $\alpha^2 F(\omega) / \omega$, we set the cutoff in the small frequency region to be 0.0005 Ry whenever such a term appeared in the integrand, and μ^* was taken to be 0.1.

We calculated the SF mediated electron-electron interaction within the adiabatic local density approximation[39, 45, 46]. In analogy to λ , the SF parameter, measuring the averaged SF strength over the Fermi surface, is defined as

$$\mu_s = \frac{1}{N(\epsilon_F)} \sum_{\mathbf{k}\mathbf{k}'n'n'} V_{n\mathbf{k}n'\mathbf{k}'}^{\text{SF}} \delta(\epsilon_{n\mathbf{k}}) \delta(\epsilon_{n'\mathbf{k}'}), \quad (11)$$

where $V_{n\mathbf{k}n'\mathbf{k}'}^{\text{SF}}$ is the effective interaction of SF, which is calculated in the following way:

$$V_{n\mathbf{k}n'\mathbf{k}'}^{\text{SF}} = \frac{2}{\pi} \int d\omega \frac{|\epsilon_{n\mathbf{k}}| + |\epsilon_{n'\mathbf{k}'}|}{(|\epsilon_{n\mathbf{k}}| + |\epsilon_{n'\mathbf{k}'}|)^2 + \omega^2} \times \Lambda_{n\mathbf{k}n'\mathbf{k}'}^{\text{SF}}(i\omega). \quad (12)$$

$\Lambda_{n\mathbf{k}n'\mathbf{k}'}^{\text{SF}}$ contains the effective interaction of SF, and can be derived from:

$$\Lambda^{\text{SF}}(\mathbf{r}, \mathbf{r}', i\omega) = - \int d\mathbf{r}_1 d\mathbf{r}_2 I^{\text{XC}}(\mathbf{r}, \mathbf{r}_1) \times \Pi(\mathbf{r}_1, \mathbf{r}_2, i\omega) I^{\text{XC}}(\mathbf{r}_2, \mathbf{r}'), \quad (13)$$

where Π is the spin susceptibility and I^{XC} denotes the second-order functional derivative of the exchange-correlation energy with respect to the spin density. See Refs. [38, 39, 46] for more information.

The Kohn-Sham (KS) self-consistent calculations for charge densities were performed on a $12 \times 12 \times 12$ \mathbf{k} grid. The uniform hole doping was realized by subtracting electrons from unit cells, and adding a compensating jellium background. Calculations of phonon energies $\omega_{\mathbf{q}\nu}$ and phonon line widths $\gamma_{\mathbf{q}\nu}$ and the electron-phonon matrix element $g_{m\nu}(\mathbf{k}, \mathbf{q})$ within the harmonic approximation (HA) were performed using the density functional perturbation theory (DFPT) scheme implemented in QUANTUM ESPRESSO (QE)[47, 48] on a $6 \times 6 \times 6$ \mathbf{q} point mesh. The \mathbf{q} grid was half-shifted in order to avoid the divergence regarding the double delta integral in Eq. (10). We used the ultra-soft pseudopotentials[49] with PBE exchange and correlation functionals[50]. The kinetic energy cutoff for wavefunctions and charge densities were set to 100 Ry and 800 Ry, respectively. The optimized tetrahedron method[51] was used to avoid broadening dependence. In the calculations of electron-phonon coupling (EPC), the derivative of the self-consistent potential was evaluated on the same \mathbf{q} grid, whereas the KS energies $\epsilon_{n\mathbf{k}}$ were computed in a non-self-consistent calculation with a $24 \times 24 \times 24$ k grid.

One approach to dealing with anharmonicity is using the self-consistent phonon method (SCPH)[52]. In this approach, one renormalizes the harmonic phonon frequencies through the phonon self-energy. We used ALAMODE[53] to do the SCPH calculations. In the SCPH calculations, we first prepared a $2 \times 2 \times 2$ supercell containing 40 atoms and generated more than 160 configurations for each system by adding random displacements between 0.05 to 0.2 Å, and calculated corresponding inter-atomic forces using QE with the same

pseudopotentials as mentioned before and a $8 \times 8 \times 8$ k -point mesh. The inter-atomic force constants (IFCs) were then fitted by the least squares method to minimize the sum of residual squares. The IFCs were fitted up to the sixth order for a robust estimation of IFCs. For the second-order IFCs, the cutoff range included the whole supercell, while for the rest the cutoff range were set to include only the nearest neighbors. The average fitting error was 0.925%. The SCPH equations were solved on a $4 \times 4 \times 4$ mesh at 0 K, and we extracted the anharmonic corrections to the second-order IFCs. With the IFCs containing anharmonic corrections, we obtained the renormalized phonon frequencies, along with the renormalized Eliashberg spectral function $\alpha^2 F(\omega)$, from which we calculated λ and ω_{log} . The dynamical stability is judged from the phonon spectral.

Superconducting T_c was finally calculated without empirical parameters on the basis of SCDFIT[54] using the superconducting toolkit[38]. The random phase approximation (RPA)[55] was applied in the computation of the screened Coulomb interaction, where the frequency dependence was retained for including the dynamical screening via the plasmon oscillation[56, 57]. The KS orbitals were calculated on a $6 \times 6 \times 6$ k mesh. When calculating the superconducting gap equation, we included 50 energy bands, and adopted the for phononic part the exchange-correlation kernel SPG2020[58].

III. RESULTS AND DISCUSSION

A. Electronic structure

In Fig. 2 we plotted the electronic band structure and projected DOS of KMgH₃, without doping, at ambient pressure. The band gap is approximately 2.4 eV, whereas the valence states are dominated by hydrogen 1s orbitals. The valence states of KMgH₃ show a peak in the electronic DOS, whose value reaches about 3.8 states $\cdot \text{eV}^{-1} \cdot \text{u.c.}^{-1}$. For comparison, the DOS at the Fermi level of $Im\bar{3}m$ H₃S under 250GPa is about 0.7 states $\cdot \text{eV}^{-1} \cdot \text{u.c.}^{-1}$ [26]. Below the Fermi level, the DOS monotonically increases, and reaches a maximum at around -2 eV relative to the Fermi level, which makes it an ideal choice for hole-doping.

B. Stability

The thermodynamical stability of the pristine KMgH₃ was confirmed by calculations of enthalpies relative to the binary hydrides KH and MgH₂ presented in Fig. 3(a). We hence assume that it can stay thermodynamically stable with small doping, especially at higher pressures. The dynamical stability of the cubic phase of doped KMgH₃ was examined by first calculating phonon frequencies within the harmonic approximation with DFPT, and checking if imaginary phonon modes appeared. These

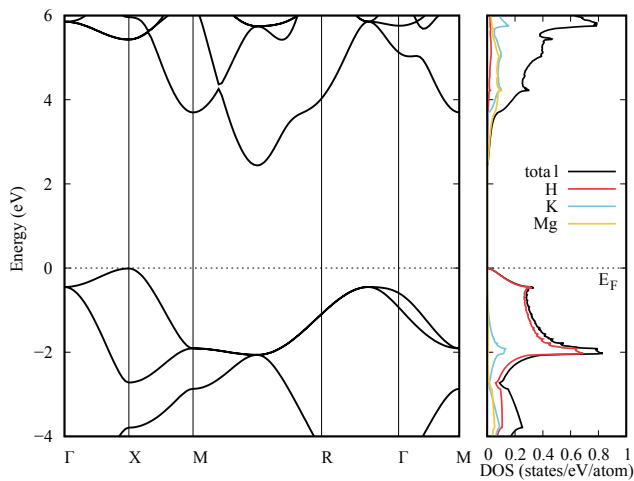


FIG. 2. Electronic bands structure and DOS of KMgH_3 before doping at ambient pressure.

harmonic phonon frequencies are further renormalized through SCPH iterations, and the ones still showing imaginary modes are deemed to be unstable.

The phase diagram of doped KMgH_3 is shown in Fig. 3(b), where doping concentration n denotes the number of electrons subtracted per unit cell. The dynamical stability gradually decreases with increasing pressure and doping concentration. Within a narrow range, lattice anharmonicity helps to restore the phase stability. Fig. 4 shows some typical phonon dispersions with both harmonic and anharmonic frequencies. The imaginary modes which appear around Γ point are hardened by anharmonicity, which indicates the dynamical stability brought about by anharmonic effects. Apart from this, the middle branches are mostly affected by anharmonicity, with a universal enhancement in frequency of 5.71% on average, while the frequency shift among the highest branches are on average only +0.43%.

The impact of pressure is most significant on the highest branches. Meanwhile, the other branches are also hardened by the increase of pressure, along with the appearance of imaginary modes in the acoustic branches. When the lattice parameter shrinks from 7.6 a.u. to 5.8 a.u., the average phonon frequencies of the three highest optical branches are strengthened from 1200 cm^{-1} to 2700 cm^{-1} . The middle branches are hardened from 600 cm^{-1} to about 1000 cm^{-1} on average. On the other hand, the impact of doping is most obvious in the middle branches, leaving the highest branches almost untouched. Similar to pressure, increasing n also tends to weaken the dynamical stability.

C. Superconductivity

For the stable systems, we performed calculations of electron-phonon coupling with the renormalized phonon frequencies. Fig. 5 contains two typical plots of Eliashberg functions. The coupling is strongest among mid-

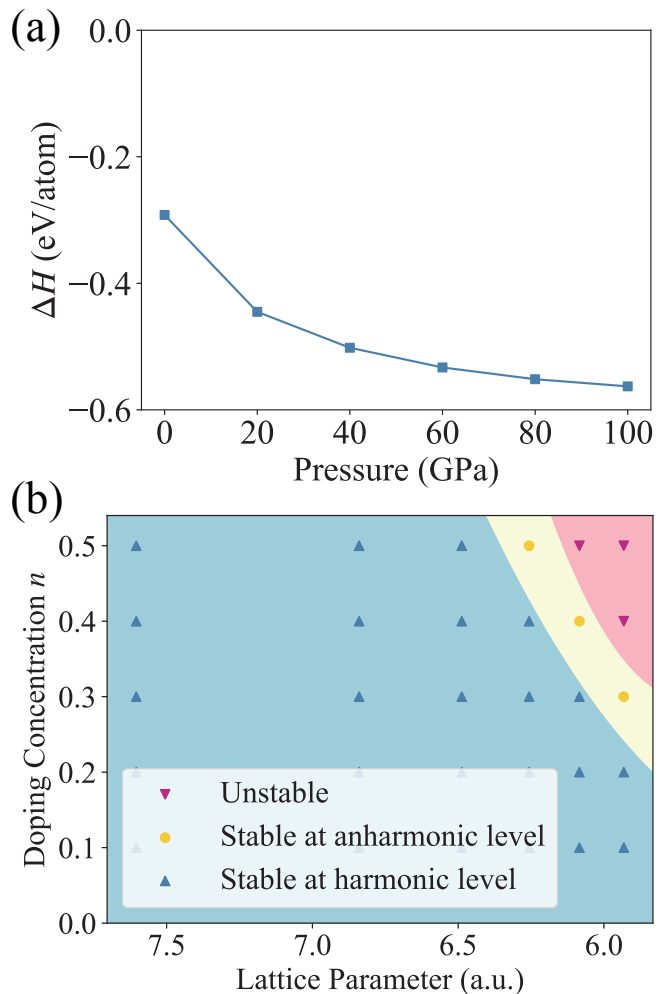


FIG. 3. (a) Calculated enthalpy difference (relative to KH in the $Fm\bar{3}m$ phase and MgH_2 in the $P4_2/mnm$ phase) of KMgH_3 from ambient pressure to 100 GPa. (b) The dynamical stability of the cubic phase of hole doped KMgH_3 with respect to doping concentration and lattice parameter. Smaller lattice parameters indicates higher pressures. A lattice parameter of 7.6 (5.8) a.u. are equal to the lattice parameter of the undoped compound under ambient (100GPa) pressure.

dle and lower frequencies, while in the high-frequency branches the coupling is negligible, indicating that such vibrations of hydrogen do not participate in EPC. Consequently, the pressure effects on λ appeared to be ambiguous in the lower doping case, since pressure mostly affects the highest branches of phonon modes, which are barely coupled with electron, and have almost no influence on λ . From Fig. 5 we see the contributions to λ almost entirely come from the middle and low branches of phonon modes.

We calculated the EPC strength λ and plotted them in Fig. 6(a). λ generally increases with the doping concentration, because the Fermi surface in this compound is brought about by doping entirely, and with more doping we can expect a larger coupling strength due to the increased $N(\epsilon_F)$. The EPC is insignificant when $n \leq 0.2$,

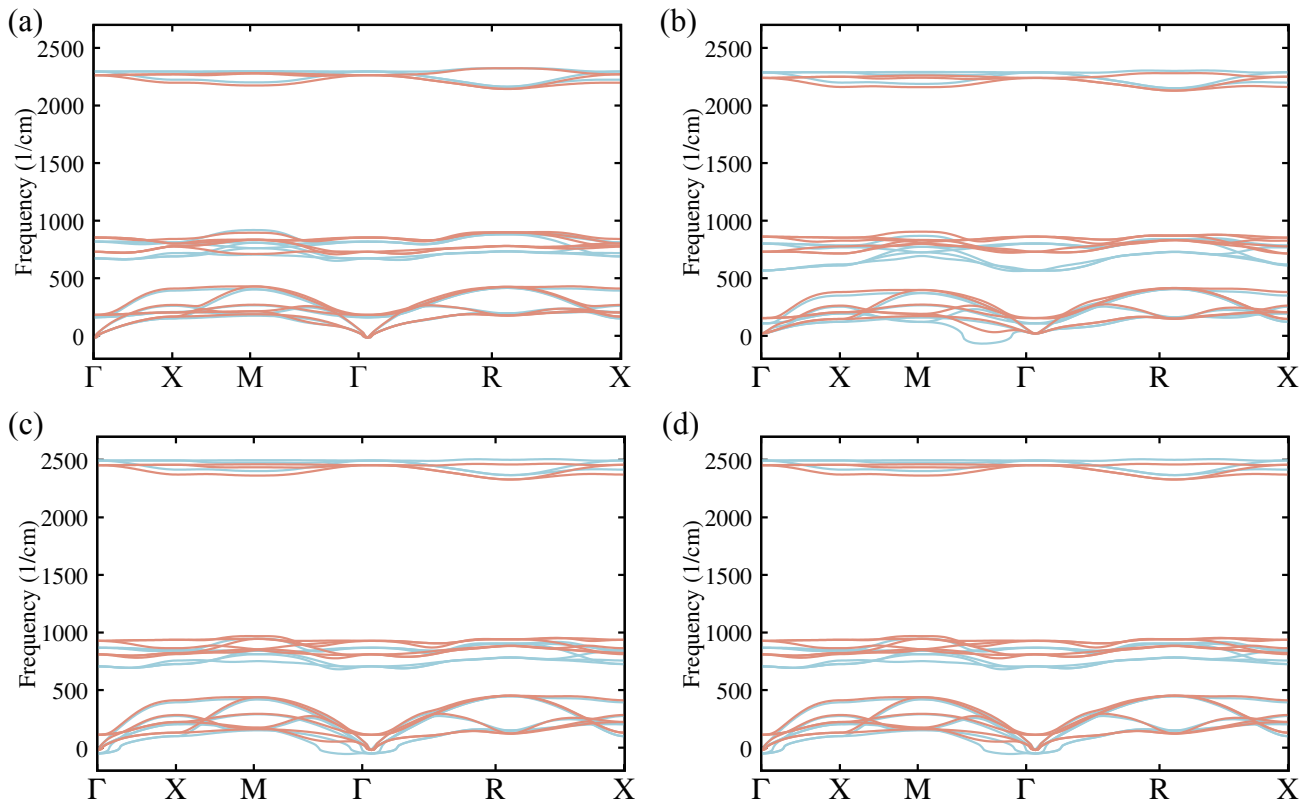


FIG. 4. Phonon dispersions of uniformly hole-doped KMgH_3 with lattice constant and doping concentration respectively equal to (a) 6.26 a.u. and 0.4. (b) 6.26 a.u. and 0.5. (c) 6.08 a.u. and 0.3. (d) 6.08 a.u. and 0.4. The blue lines are the harmonic frequencies, and the red lines are the anharmonic phonon frequencies from SCPH.

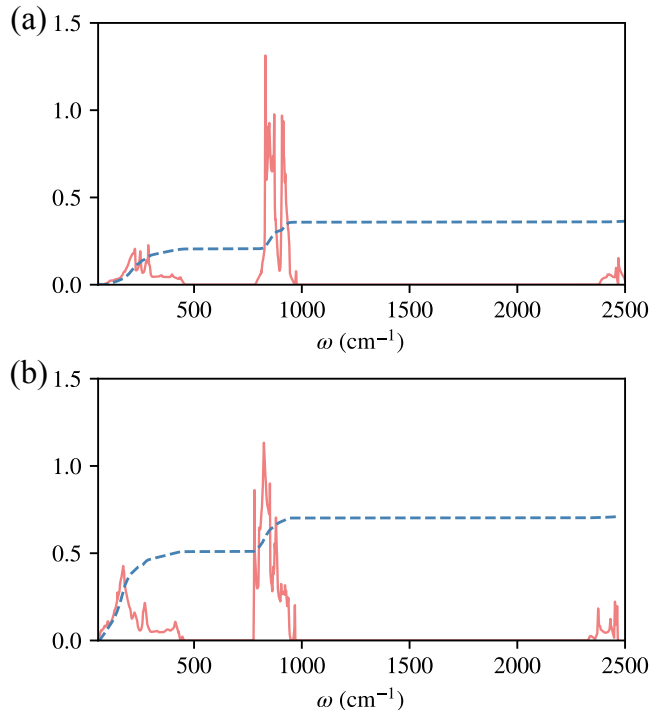


FIG. 5. The Eliashberg spectral functions when lattice constant is 6.08 a.u., and doping concentration is (a) 0.3. (b) 0.4. The red solid lines are the spectral functions, and the blue dashed lines are integrated value of λ .

only giving λ 's mostly smaller than 0.2. Therefore, we do not expect superconductivity from this small doping region. The strongest coupling happens when $a = 6.26$ a.u. and $n = 0.5$, where λ reaches 0.72. Overall, the hole-doped KMgH_3 is far from a strong coupling material as we have expected. Furthermore, by including lattice anharmonicity, λ is slightly decreased. Such suppression of EPC in hydrides due to anharmonicity is in qualitative agreement with previous researches[26, 29]. This is because the hardening moves the coupling phonon frequencies farther from the optimal regime of $\sim 7T_c$ [59–61].

Transition temperatures were estimated from Eq. (2) for the stable systems whose λ is no less than 0.1, and the results are plotted in Fig. 6(b). We see that there is almost no superconductivity found for $n \leq 0.3$ except at high pressure ($a = 5.8$ a.u. and $n = 0.3$), as a result of minor $N(\epsilon_F)$ values. Just like λ , T_c benefits from the larger $N(\epsilon_F)$ rise by the increasing doping concentration. The highest T_c (K) occurs under the conditions where $a = 6.26$ a.u. and $n = 0.5$, which would have been considered unstable if only treated within HA.

In order to get rid of the arbitrariness brought about by the empirical choice of μ^* , we also performed SCDFC calculations for all the systems. Fig. 6(c) and Fig. 6(d) compare transition temperatures predicted from SCDFC without and with SF. Without SF, the general trends in T_c qualitatively agree with those in the T_c from MAD,

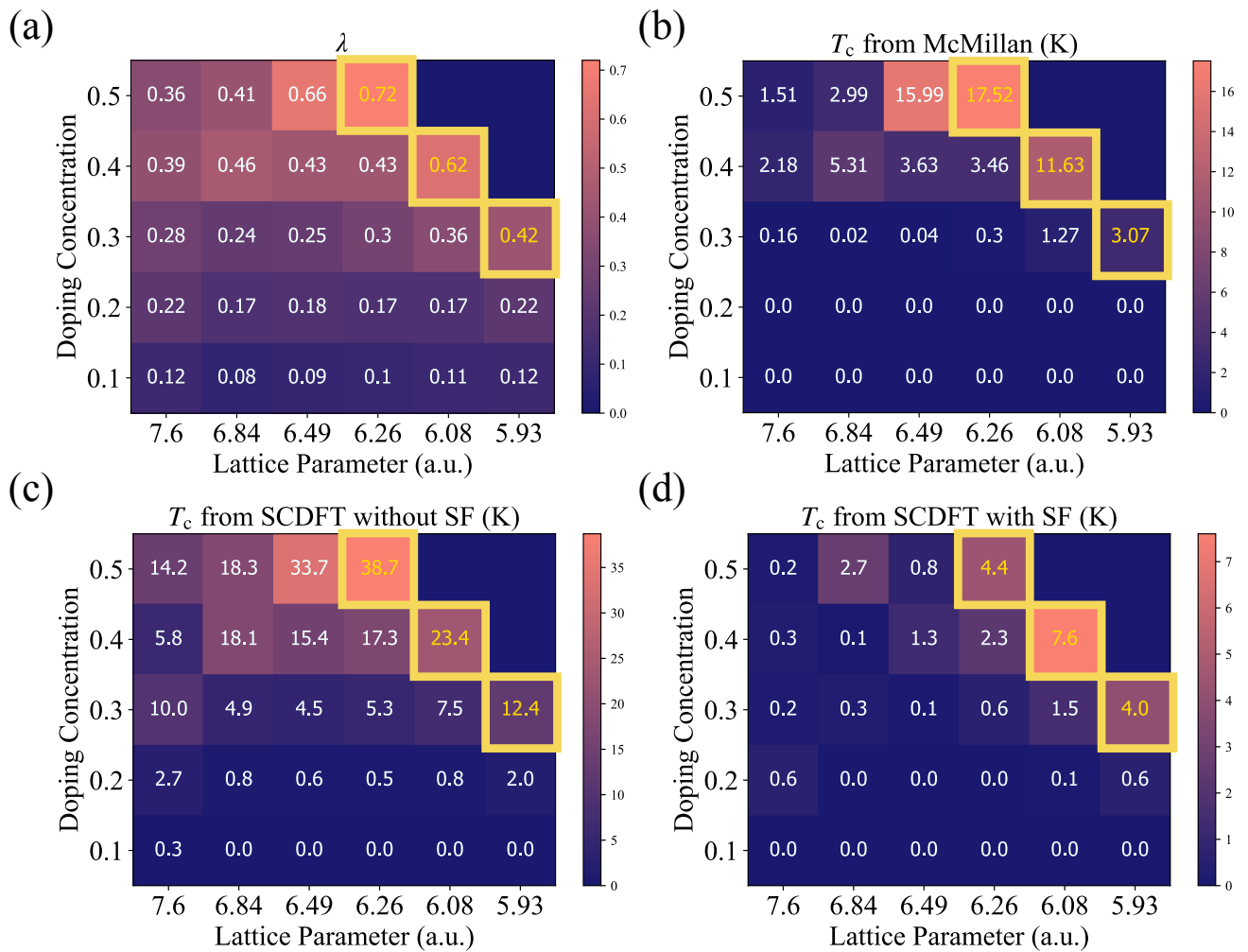


FIG. 6. Lattice constant and doping concentration dependence of (a) EPC parameter λ . (b) T_c estimated from MAD formula with $\mu^* = 0.1$. (c) T_c predicted from SCDFT without SF. (d) T_c predicted from SCDFT with SF included. The highlighted parts indicate the ones that are only stable at anharmonic level.

because in both cases only phonon and Coulomb contributions were treated. The inclusion of SF caused a substantial decrease in T_c . The highest transition temperature no longer happens when the lattice parameter is 6.26 *a.u.* and n is 0.5; for that point T_c drops from 38.7 K to only 4.4 K. Overall, the highest T_c becomes 7.6 K. The reduction of T_c indicates a strong SF in the doped KMgH_3 , which could result from the localized electrons orbitals[39]. In Fig. 7(a), we plotted the electron localization functions within the Mg-H plane for doped KMgH_3 . Despite the doping and the applied pressure, the electronic orbitals are still largely localized, contributing to a considerable part of the magnetic exchange-correlation kernel, which results in a lower T_c . In comparison, a plot of ELF for $Im\bar{3}m$ H_3S in the (1, 0, 0) plane is shown in Fig. 7(b). The electrons are well delocalized between S atoms and their nearest H atoms, which may explain the minor reduction on T_c from 203 K to 190 K due to SF in H_3S [62]. By applying pressure or increasing doping concentration, it is possible to enhance T_c through increasing

the EPC strength and lowering the SF effect, because of the more overlapped orbitals. However, maintaining the phase stability under such a situation could be a difficult problem.

Interestingly, compared with neighboring systems stable within HA, T_c was enhanced in all systems stabilized by anharmonic effects where the possibility of superconductivity is usually not considered. The present calculations suggest the possibility of discovering new superconductors in such systems stabilized by the anharmonic effect.

D. Spin fluctuation

In this subsection we dwell more into the possible origin of such strong SF effects in the doped KMgH_3 .

In Fig. 8, we plotted the correlation between the SF strength μ_s , defined in Eq. 11, and $N(\epsilon_F)$. In this figure, we include all the stable phases of doped KMgH_3 . To confirm the generality of the trend, we also calculated μ_s

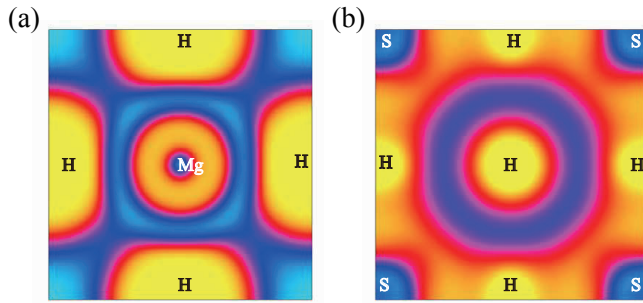


FIG. 7. Electron localization function of (a) KMgH_3 , where lattice constant is 6.26 a.u. and doping concentration is 0.5, in the Mg-H plane. (b) $Im\bar{3}m$ H_3S . The cyan, magenta, and yellow colours represent high, medium, and low density, respectively. The two figures are made with VESTA[63].

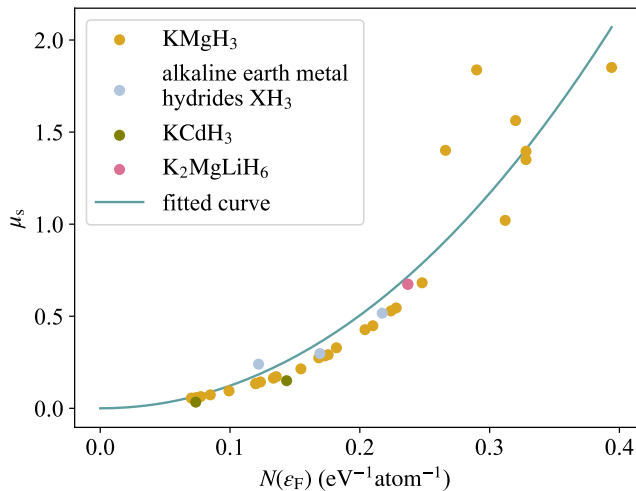


FIG. 8. SF strength μ_s with respect to the DOS at the Fermi level $N(\epsilon_F)$. The solid circles are all the stable doped KMgH_3 , alkaline earth metal hydrides XH_3 , X being Mg, Ca and Sr, perovskite hydride KCdH_3 before and after doping, and Li-doped KMgH_3 , respectively. The solid line is the fitted curve according to Eq. (15).

of other hydrides having valence states formed almost exclusively by H-1s orbitals, either stable or unstable[64]. This feature is rarely seen in experimentally confirmed or theoretically predicted hydride superconductors, since the H-1s bands usually only make a small contribution to the total $N(\epsilon_F)$. If we assume that the spin-spin interaction is constant, the effective interaction averaged over the Fermi surface can be estimated as:

$$V_{nkn'\mathbf{k}'}^{\text{SF}} \approx \frac{s_1 N(\epsilon_F)}{1 - s_2 N(\epsilon_F)}, \quad (14)$$

where s_1 and s_2 are constants among the same type of hydrides. Combining Eq. (14) and (11), we have the following approximation

$$\mu_s \approx \frac{s_1 N(\epsilon_F)^2}{1 - s_2 N(\epsilon_F)}. \quad (15)$$

In materials like doped KMgH_3 , μ_s grows substantially when the $N(\epsilon_F)$ becomes larger, and the correlation can still be well fitted to Eq. (15), in spite of the crude approximation. The largest μ_s can reach as high as 1.85. Since doped KMgH_3 is only a medium to low coupling superconductor, such μ_s is expected to largely reduce T_c , or suppress superconductivity completely even at low $N(\epsilon_F)$, because λ is also approximately proportional to $N(\epsilon_F)$. When μ_s is close or even larger than λ , T_c could be greatly or even completely suppressed (e.g., in elemental scandium)[38], which is what happens in the case of doped KMgH_3 .

This phenomenon indicates a possible dilemma for hydride superconductors. While one attempts to make use of the H-1s orbitals in hydride superconductors to seek a strong EPC, such hydrides will possibly suffer from the suppression of T_c resulted from large SF effects.

IV. SUMMARY

We have examined the superconducting properties, including the EPC strength, SF effects, and superconducting transition temperature, of uniformly hole-doped perovskite hydride KMgH_3 under varying doping concentration and lattice parameters, with lattice anharmonicity included. The highest T_c predicted by SCDFT is 7.6 K. The suppressed T_c indicates that the doped KMgH_3 could be an interesting material where strong SF effects are expected, which reduce T_c . The exceptional suppression of superconductivity caused by SF could also be expected to happen in other hydride superconductors, where the hydrogen 1-s bands are isolated at the Fermi level, which calls for additional attention in the current search for hydride superconductors. We also found that T_c is enhanced when the system is on the edge of stability and is stabilized by lattice anharmonicity. Along with the suppression effects of anharmonicity on T_c , our finding again emphasizes the important role of lattice anharmonicity in the study of hydride superconductors.

ACKNOWLEDGMENTS

We would like to express our gratitude to Dr. Terumasa Tadano, Dr. Takahiro Ishikawa and Dr. Tomohito Amano for enlightening discussions and valuable suggestions. The calculations in this research were carried out on the supercomputer Ohtaka of Institute of Solid State Physics, The University of Tokyo. This work was supported by JSPS KAKENHI Grant No. 23K03313 from Japan Society for the Promotion of Science (JSPS).

- [1] V. L. Ginzburg, *J. Stat. Phys.* **1**, 3 (1969).
- [2] N. W. Ashcroft, *Phys. Rev. Lett.* **21**, 1748 (1968).
- [3] N. W. Ashcroft, *Phys. Rev. Lett.* **92**, 187002 (2004).
- [4] A. P. Drozdov, M. I. Erements, I. A. Troyan, V. Ksenofontov, and S. I. Shylin, *Nature* **525**, 73–76 (2015).
- [5] M. Somayazulu, M. Ahart, A. K. Mishra, Z. M. Geballe, M. Baldini, Y. Meng, V. V. Struzhkin, and R. J. Hemley, *Phys. Rev. Lett.* **122**, 027001 (2019).
- [6] A. P. Drozdov, P. P. Kong, V. S. Minkov, S. P. Besedin, M. A. Kuzovnikov, S. Mozaffari, L. Balicas, F. F. Balakirev, D. E. Graf, V. B. Prakapenka, E. Greenberg, D. A. Knyazev, M. Tkacz, and M. I. Erements, *Nature* **569**, 528–531 (2019).
- [7] I. A. Troyan, D. V. Semenov, A. G. Kvashnin, A. V. Sadakov, O. A. Sobolevskiy, V. M. Pudalov, A. G. Ivanova, V. B. Prakapenka, S. Chariton, *et al.*, *Advanced Materials* **33** (2021), 10.1002/adma.202006832.
- [8] P. Kong, V. S. Minkov, M. A. Kuzovnikov, A. P. Drozdov, S. P. Besedin, S. Mozaffari, L. Balicas, F. F. Balakirev, V. B. Prakapenka, S. Chariton, D. A. Knyazev, E. Greenberg, and M. I. Erements, *Nature Communications* **12** (2021), 10.1038/s41467-021-25372-2.
- [9] Y. He, J. Lu, X. Wang, and J. Shi, *Phys. Rev. B* **108**, 054515 (2023).
- [10] A. Sanna, T. F. T. Cerqueira, Y. Fang, I. Errea, A. Ludwig, and M. A. L. Marques, *npj Computational Materials* **10** (2024), 10.1038/s41524-024-01214-9.
- [11] J. Bardeen, L. N. Cooper, and J. R. Schrieffer, *Phys. Rev.* **108**, 1175 (1957).
- [12] T. F. T. Cerqueira, A. Sanna, and M. A. L. Marques, *Advanced Materials* (2023), 10.1002/adma.202307085.
- [13] K. Choudhary and K. Garrity, *npj Computational Materials* **8** (2022), 10.1038/s41524-022-00933-1.
- [14] A. M. Shipley, M. J. Hutcheon, R. J. Needs, and C. J. Pickard, *Phys. Rev. B* **104**, 054501 (2021).
- [15] D. Wines, K. Choudhary, A. J. Biacchi, K. F. Garrity, and F. Tavazza, *Nano Letters* **23**, 969–978 (2023).
- [16] H. Yagyu, M. Kato, T. Noji, and Y. Koike, *Physics Procedia* **45**, 109 (2013), proceedings of the 25th International Symposium on Superconductivity (ISS2012).
- [17] T. F. T. Cerqueira, A. Sanna, and M. A. L. Marques, *Advanced Materials* **36**, 2307085 (2024).
- [18] R. Schumacher and A. Weiss, *Journal of the Less Common Metals* **163**, 179 (1990).
- [19] M. Ghim, N. Sato, R. Akashi, S. Jhi, and S. Tsuneyuki, *Phys. Rev. Mater.* **5**, 054802 (2021).
- [20] Y. Goto, C. Tassel, Y. Noda, O. Hernandez, C. J. Pickard, M. A. Green, H. Sakaebe, N. Taguchi, Y. Uchimoto, Y. Kobayashi, and H. Kageyama, *Inorganic Chemistry* **56**, 4840–4845 (2017).
- [21] F. D. Romero, A. Leach, J. S. Möller, F. Foronda, S. J. Blundell, and M. A. Hayward, *Angewandte Chemie* **126**, 7686–7689 (2014).
- [22] C. Tassel, Y. Goto, Y. Kuno, J. Hester, M. Green, Y. Kobayashi, and H. Kageyama, *Angewandte Chemie International Edition* **53**, 10377–10380 (2014).
- [23] Y. Sasahara, R. Terada, H. Ubukata, M. Asahi, D. Kato, T. Tsumori, M. Namba, Z. Wei, C. Tassel, and H. Kageyama, *Journal of the American Chemical Society* **146**, 11694–11701 (2024).
- [24] K. Nasu, *Phys. Rev. B* **44**, 7625 (1991).
- [25] C. C. Yu and P. W. Anderson, *Phys. Rev. B* **29**, 6165 (1984).
- [26] W. Sano, T. Koretsune, T. Tadano, R. Akashi, and R. Arita, *Phys. Rev. B* **93**, 094525 (2016).
- [27] I. Errea, M. Calandra, and F. Mauri, *Phys. Rev. Lett.* **111**, 177002 (2013).
- [28] I. Errea, M. Calandra, C. J. Pickard, J. Nelson, R. J. Needs, Y. Li, H. Liu, Y. Zhang, Y. Ma, and F. Mauri, *Phys. Rev. Lett.* **114**, 157004 (2015).
- [29] P. Hou, F. Belli, R. Bianco, and I. Errea, *Phys. Rev. B* **103**, 134305 (2021).
- [30] B. N. Ganguly, *Zeitschrift für Physik A Hadrons and nuclei* **265**, 433–439 (1973).
- [31] J. M. Rowe, J. J. Rush, J. E. Schirber, and J. M. Mintz, *Phys. Rev. Lett.* **57**, 2955 (1986).
- [32] B. M. Klein and R. E. Cohen, *Phys. Rev. B* **45**, 12405 (1992).
- [33] I. Errea, F. Belli, L. Monacelli, A. Sanna, T. Koretsune, T. Tadano, R. Bianco, M. Calandra, R. Arita, F. Mauri, and J. A. Flores-Livas, *Nature* **578**, 66–69 (2020).
- [34] I. Errea, M. Calandra, C. J. Pickard, J. R. Nelson, R. J. Needs, Y. Li, H. Liu, Y. Zhang, Y. Ma, and F. Mauri, *Nature* **532**, 81–84 (2016).
- [35] N. F. Berk and J. R. Schrieffer, *Phys. Rev. Lett.* **17**, 433 (1966).
- [36] M. A. Jensen and K. Andres, *Journal of Applied Physics* **38**, 1255 (1967).
- [37] H. Rietschel and H. Winter, *Phys. Rev. Lett.* **43**, 1256 (1979).
- [38] M. Kawamura, Y. Hizume, and T. Ozaki, *Phys. Rev. B* **101**, 134511 (2020).
- [39] K. Tsutsumi, Y. Hizume, M. Kawamura, R. Akashi, and S. Tsuneyuki, *Phys. Rev. B* **102**, 214515 (2020).
- [40] G. M. Eliashberg, *Soviet Physics JETP* **11**, 696 (1960).
- [41] A. B. Migdal, *Soviet Physics JETP* **7**, 996 (1958).
- [42] W. L. McMillan, *Phys. Rev.* **167**, 331 (1968).
- [43] P. B. Allen and R. C. Dynes, *Phys. Rev. B* **12**, 905 (1975).
- [44] R. Dynes, *Solid State Communications* **10**, 615 (1972).
- [45] M. Petersilka, U. J. Gossmann, and E. K. U. Gross, *Phys. Rev. Lett.* **76**, 1212 (1996).
- [46] F. Essenberg, A. Sanna, A. Linscheid, F. Tandetzy, G. Profeta, P. Cudazzo, and E. K. U. Gross, *Phys. Rev. B* **90**, 214504 (2014).
- [47] P. Giannozzi, S. Baroni, N. Bonini, M. Calandra, R. Car, C. Cavazzoni, D. Ceresoli, G. L. Chiarotti, M. Cococcioni, I. Dabo, *et al.*, *Journal of Physics: Condensed Matter* **21**, 395502 (2009).
- [48] P. Giannozzi, O. Andreussi, T. Brumme, O. Bunau, M. B. Nardelli, M. Calandra, R. Car, C. Cavazzoni, D. Ceresoli, *et al.*, *Journal of Physics: Condensed Matter* **29**, 465901 (2017).
- [49] D. Vanderbilt, *Phys. Rev. B* **41**, 7892 (1990).
- [50] J. P. Perdew, K. Burke, and M. Ernzerhof, *Phys. Rev. Lett.* **77**, 3865 (1996).
- [51] M. Kawamura, Y. Gohda, and S. Tsuneyuki, *Phys. Rev. B* **89**, 094515 (2014).
- [52] T. Tadano and S. Tsuneyuki, *Phys. Rev. B* **92**, 054301 (2015).
- [53] T. Tadano, Y. Gohda, and S. Tsuneyuki, *Journal of Physics: Condensed Matter* **26**, 225402 (2014).

- [54] M. Lüders, M. A. L. Marques, N. N. Lathiotakis, A. Floris, G. Profeta, L. Fast, A. Continenza, S. Massidda, and E. K. U. Gross, *Phys. Rev. B* **72**, 024545 (2005).
- [55] M. Gell-Mann and K. A. Brueckner, *Phys. Rev.* **106**, 364 (1957).
- [56] Y. Takada, *Journal of the Physical Society of Japan* **45**, 786–794 (1978).
- [57] R. Akashi and R. Arita, *Phys. Rev. Lett.* **111**, 057006 (2013).
- [58] A. Sanna, C. Pellegrini, and E. K. U. Gross, *Phys. Rev. Lett.* **125**, 057001 (2020).
- [59] G. Bergmann and D. Rainer, *Zeitschrift für Physik* **263**, 59–68 (1973).
- [60] K. Tanaka, J. S. Tse, and H. Liu, *Phys. Rev. B* **96**, 100502 (2017).
- [61] R. Akashi, R. Arita, C. Zhang, K. Tanaka, and J. S. Tse, *Phys. Rev. B* **103**, 134517 (2021).
- [62] R. Koshiji, M. Fukuda, M. Kawamura, and T. Ozaki, *Phys. Rev. Mater.* **6**, 114802 (2022).
- [63] K. Momma and F. Izumi, *Journal of Applied Crystallography* **44**, 1272 (2011).
- [64] See Supplemental Material at URL-will-be-inserted-by-publisher for more detailed information, which also includes Refs. [65–70].
- [65] G. Kresse and J. Furthmüller, *Computational Materials Science* **6**, 15 (1996).
- [66] G. Kresse and J. Hafner, *Phys. Rev. B* **47**, 558 (1993).
- [67] G. Kresse and D. Joubert, *Phys. Rev. B* **59**, 1758 (1999).
- [68] G. Kresse and J. Furthmüller, *Phys. Rev. B* **54**, 11169 (1996).
- [69] M. van Setten, M. Giantomassi, E. Bousquet, M. Verstraete, D. Hamann, X. Gonze, and G.-M. Rignanese, *Computer Physics Communications* **226**, 39 (2018).
- [70] D. R. Hamann, *Phys. Rev. B* **88**, 085117 (2013).

Supplementary Materials

A. Doped KMgH_3

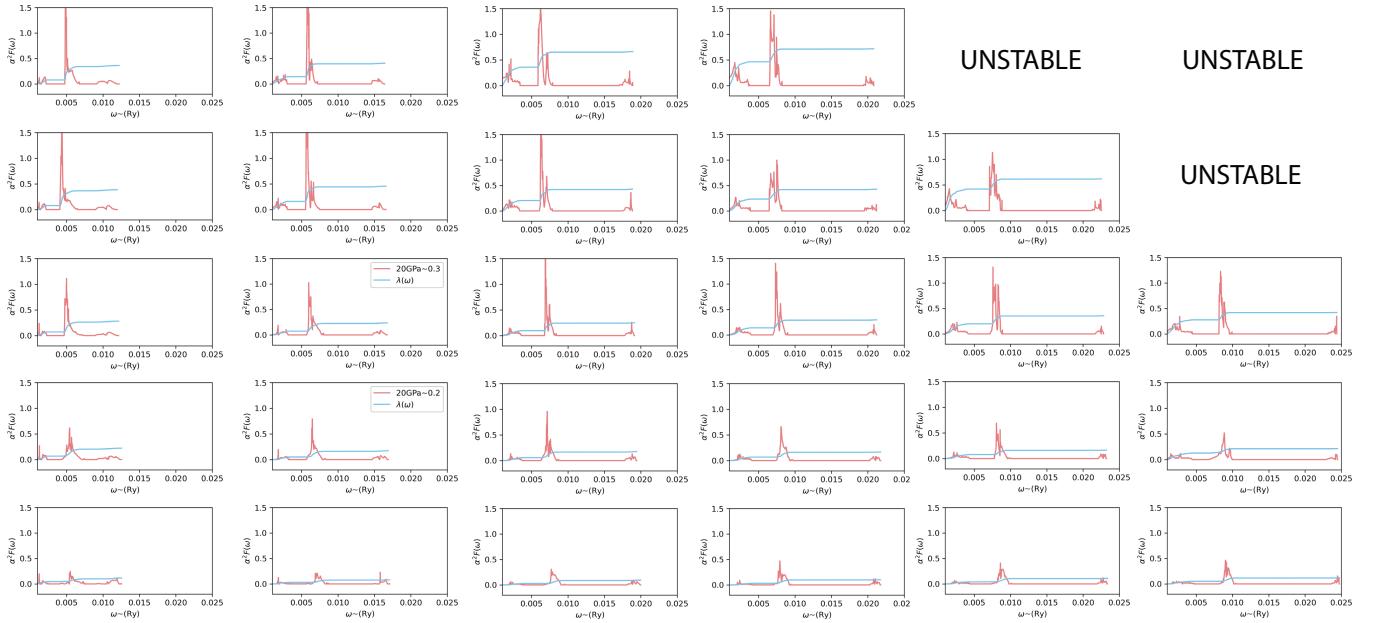


FIG. S-1. The Eliashberg spectral functions $\alpha^2 F(\omega)$ and the electron-phonon coupling parameter λ . The red lines indicate the $\alpha^2 F(\omega)$, and the blue lines are integrated λ . Columns from left to right correspond to lattice parameters of 7.60, 6.84, 6.49, 6.26, 6.08 and 5.93 bohr. Rows from bottom to top correspond to doping concentrations of 0.1, 0.2, 0.3, 0.4 and 0.5.

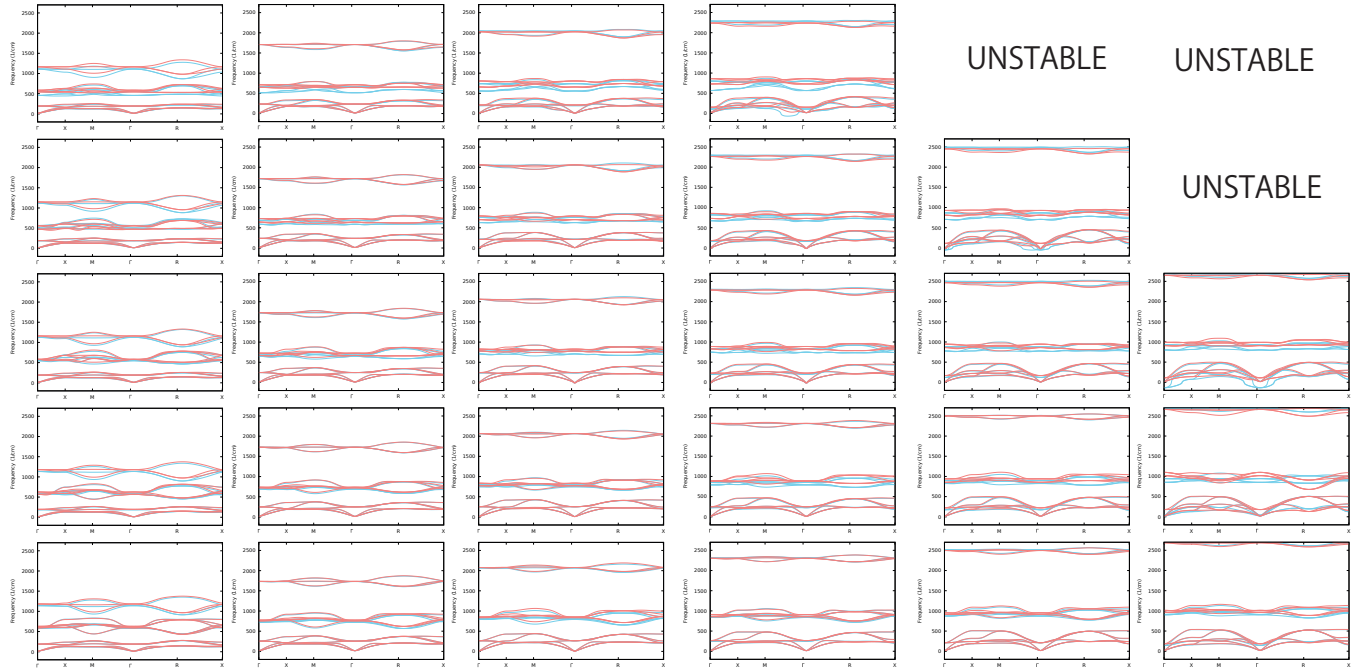


FIG. S-2. Phonon dispersions of doped KMgH_3 . The red blue lines are phonon frequencies calculated within harmonic approximation. The blue lines are anharmonic phonon frequencies obtained from self-consistent phonon (SCPH) calculations. The ordering is the same as in Fig. S-1.

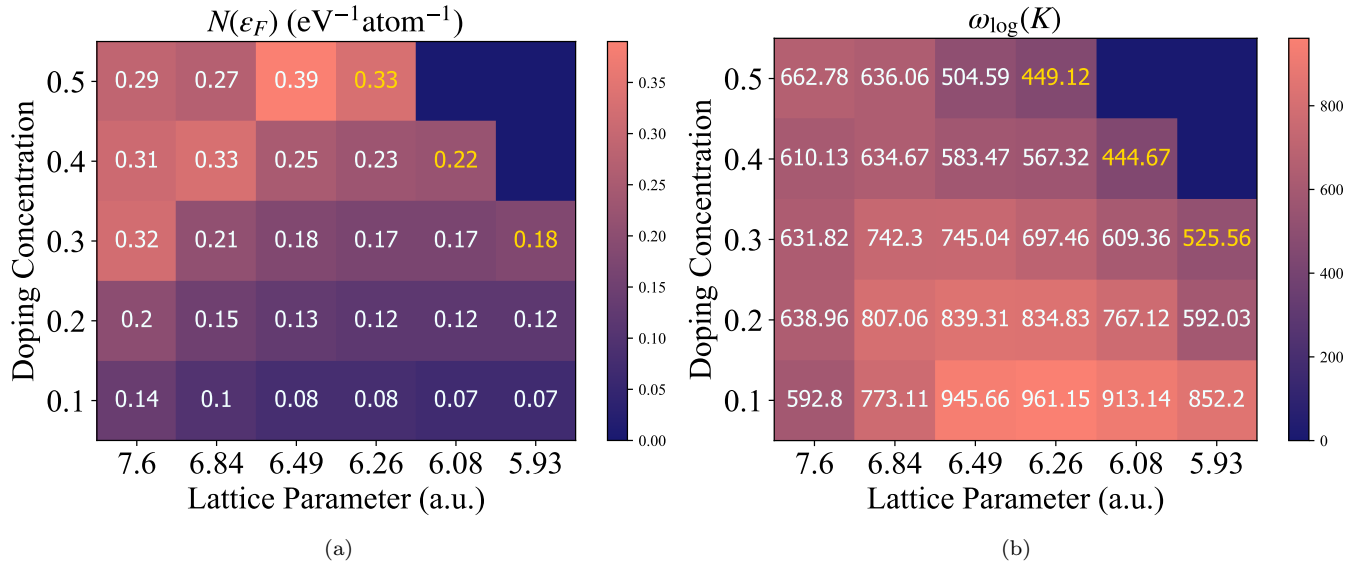


FIG. S-3. (a) Electronic density of states at the Fermi level $N(\epsilon_F)$. (b) Logarithmic average of phonon frequencies ω_{\log} of doped KMgH_3 .

B. K_2LiMgH_6

K_2LiMgH_6 is a lithium-doped KMgH_3 , which corresponds to a doping concentration of 0.5, where half of the Mg atoms are replaced by lithium atoms. The crystal structure was optimized using the Vienna Ab Initio Simulation Package (VASP) [65–68] with a $12 \times 12 \times 12$ k grid under 35 GPa. Its transition temperature (T_c) was predicted, from SCDF, to be 18.2 K (without spin fluctuation (SF)) and 0.7 K (with SF).

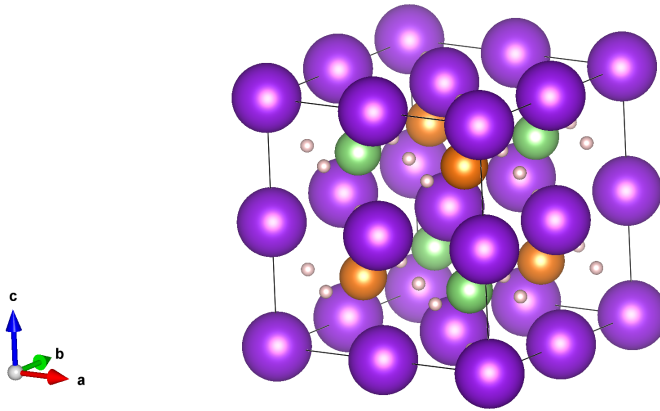
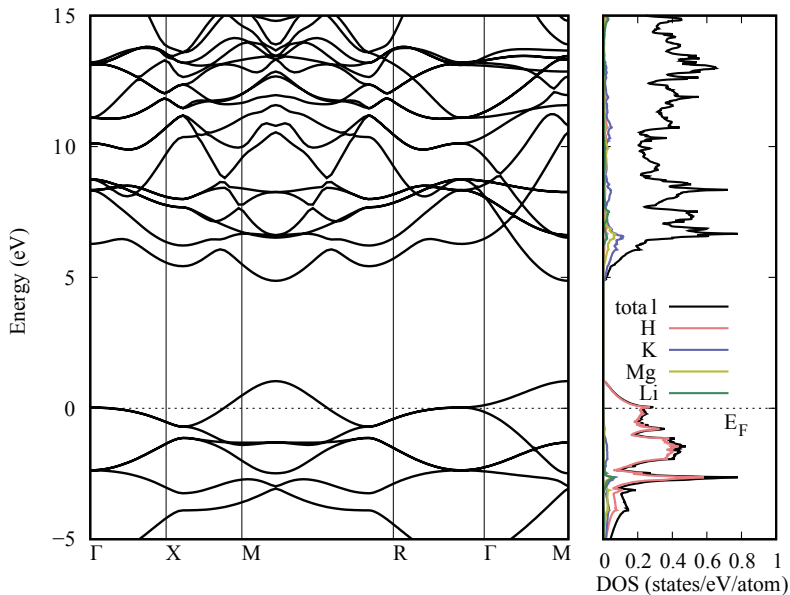


FIG. S-4. Crystal structure of K_2LiMgH_6 . The purple, green, orange, and pink balls are potassium, lithium, magnesium and hydrogen atoms, respectively.

FIG. S-5. Electronic bands structure of K_2LiMgH_6 .

$Fm\bar{3}m$ at 35 GPa			
a, b, c [Å]	6.288552	6.288552	6.288552
α, β, γ	90	90	90
H (24e)	0.26059	0.50000	0.50000
Li (4b)	0.50000	0.50000	0.50000
K (8c)	0.25000	0.25000	0.25000
Mg (4a)	0.50000	0.00000	0.50000

TABLE S-1. Calculated structure parameters for K_2LiMgH_6 .

C. Alkaline earth metal hydrides

The alkaline earth metal hydrides XH_3 do not possess dynamical stability at ambient pressure. Nevertheless, we can still estimate μ_s of them, since μ_s do not depend on phononic properties in the current scheme. They are all in the same $Fm\bar{3}m$ space group, and the lattice parameters are 4.71 Å, 5.28 Å, and 5.69 Å, for X being Mg, Ca and Sr, respectively. The X atom is in 4a Wyckoff position and the coordinates are (0.00, 0.00, 0.00). The first H atom is in 4b Wyckoff position and the coordinates are (0.50, 0.00, 0.00), and another H is in 8c Wyckoff position with its coordinates being (0.25, 0.25, 0.75). Calculated values of μ_s are listed in Table. S-2.

	$N(\epsilon_F)$ [$\text{eV}^{-1}\text{atom}^{-1}$]	μ_s
MgH_3	0.122	0.24
CaH_3	0.169	0.30
SrH_3	0.217	0.52
K_2LiMgH_6	0.237	0.67
KCdH_3	0.074	0.034
KCdH_3 (doped)	0.144	0.15

TABLE S-2. Calculated $N(\epsilon_F)$ and the strength of μ_s . The doped KCdH_3 is doped with 0.5 holes per unit cell.

D. Extra computational details

The enthalpy calculations were performed using VASP, with a $12 \times 12 \times 12$ \mathbf{k} point mesh. The energy bands that are used in the plots of electronic band structures were calculated with a $12 \times 12 \times 12$ \mathbf{k} grid with the Marzari-Vanderbilt-DeVita-Payne smearing method, and the broadening was set to be 0.005 Ry. Electronic energies used in calculations for DOS and in SCDFD for μ_s were calculated on a $16 \times 16 \times 16$ \mathbf{k} grid in a non-self-consistent way using the charge

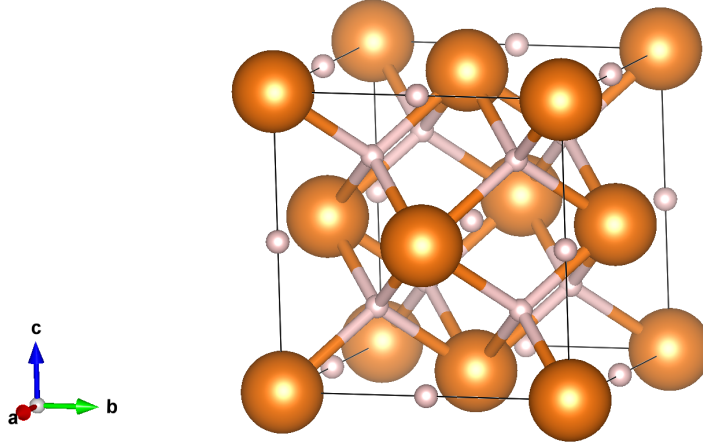


FIG. S-6. The crystal structure of $Fm\bar{3}m$ XH_3 . The orange balls are X atoms, and the pink balls are H atoms.

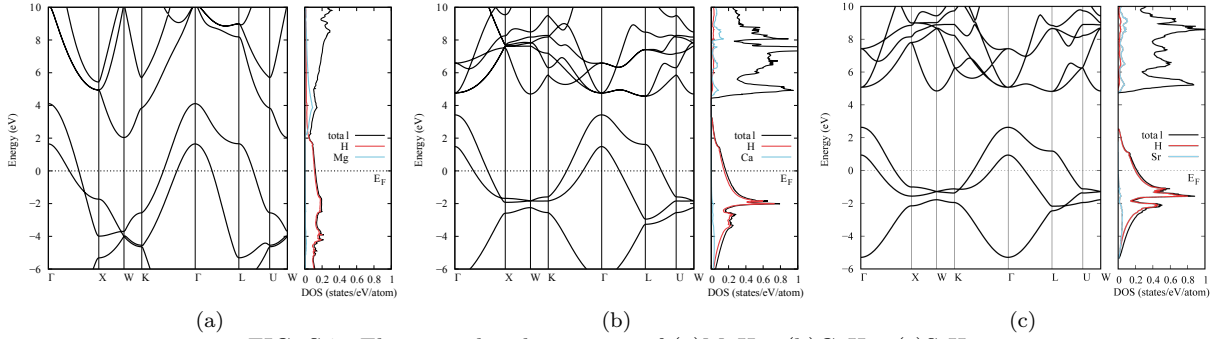


FIG. S-7. Electronic band structure of (a) MgH_3 . (b) CaH_3 . (c) SrH_3 .

densities from self-consistent calculations with $12 \times 12 \times 12$ \mathbf{k} grids, and the optimized tetrahedron method were adopted in these calculations. Norm-conserved pseudopotentials [69, 70] with PBE exchange-correlation functionals were used. The exchange integrals of SF interactions were evaluated on a $4 \times 4 \times 4$ mesh. Crystal structures shown in this article are produced by VESTA[63].